# Combining Satellite and Radar Data for the Short-Range Forecasting of Precipitation

A. BELLON, S. LOVEJOY AND G. L. AUSTIN

*Stormy Weather Group, McGill University, Montreal, Canada*

(Manuscript received 1 April 1979, in final form 27 May 1980)

ABSTRACT

An algorithm yielding probability of rain from GOES visible-infrared imagery and simultaneous radar data is applied over a satellite image the size of eastern Canada. It is then mapped by means of a conic projection on a constant resolution Cartesian grid to facilitate overlay with synoptic charts. A pattern recognition technique is applied to 16 subareas of the entire map and has proved successful in tracking the displacement of the probability-of-rain contours. The potential of the system for making short-range precipitation forecasts is discussed briefly.

## 1. Introduction

Steady progress in the skill of numerical weather prediction has been achieved during the past 20 years, resulting in improved forecasting in the 12 h and longer time scales. The forecasting, particularly of precipitation, in the 0–6 h domain, however, has shown no significant advance and, indeed, is usually given to the public only in general terms (e.g., Sanders, 1979). We believe that not only is there a great need for improvements in this type of forecast for aviation, urban hydrology and agriculture but also that, by rapid dissemination via television, the general public would appreciate accurate rain predictions a few hours ahead. While it is possible to hope for these predictions to become available from regional fine-mesh numerical models, we expect that improvement in the 0–6 h domain lies in the combination of satellite and radar data, since only these data have the necessary spatial and temporal resolution. Work on mesoscale numerical models should still be encouraged, not only for the increase in knowledge they provide on mesoscale processes but also because the ultimate short-range forecasting strategy probably requires a combination of image processing and numerical weather prediction procedures. A possible scenario for the combining of these two apparently diverse techniques was recently described by Browning (1979).

Work at McGill has until recently concentrated on the forecasting of precipitation for the 0–3 h interval using a single weather radar. Designed largely for the terminal severe weather problem of aviation, this procedure called SHARP (SHort-term Automated Radar Prediction) was described in Austin and Bellon (1974) and Bellon and Austin (1978). Extension to longer time intervals necessitated a much larger areal coverage, on account of the significant movements of the rain areas. For eastern Canada, a network of 20 or more radars could have been set up to deal with the problem, but significant oceanic areas would still not be covered. For this reason, the delineation of rain areas from satellite imagery constituted the obvious solution.

Although this paper is not specifically directed toward rain amount estimation from satellite imagery, research in that field is relevant to the present problem. A comprehensive review of satellite rainfall estimation methods up to 1973 was gathered by Martin and Scherer (1973). More recently, Stout *et al.* (1979) and Griffith *et al.* (1978) used cumulonimbus life history techniques in refining rainfall measurements. Scofield and Oliver (1977) derived a procedure in the form of a flow diagram (decision tree) involving a visual examination of the rate of anvil growth, merging cells and overshooting tops from enhanced IR images in order to derive an appropriate rainfall rate associated with cumulonimbus clouds. Reynolds and Smith (1979) extended their technique by using remapped satellite with radar, raingage and synoptic data. Since most of the above techniques were tested on regions of convective activity particularly in the tropics, Wylie (1979) attempted with some success to apply them to a nontropical area, namely, the Montreal region.

Of significant importance are the concluding remarks of the review paper by Martin and Scherer (1973): "Based on bivariate frequency distribution of brightness versus temperature, Gruber (1973) concluded that brightness enhancing or infrared technique alone may be inadequate to deduce details of convective activity. . . . This implies that better estimates of rainfall will come from visible and IR observations *combined* than from either used alone."

0027-0644/80/101554-13$07.25

However, with the exception of a note on image differencing by Reynolds *et al.* (1978), this recommendation had not been acted on until the two-wavelength pattern-recognition technique of Lovejoy and Austin (1979a) was introduced.

Unlike the techniques of other researchers which require, to a greater or lesser degree, the need of human intervention [e.g., Stout *et al.* (1979) and particularly Scofield and Oliver (1977)] and which concentrated primarily on regions of active convection, the goal of this work is to develop a fully automated rain-delineation procedure which includes all types of precipitation. The basic algorithm toward this aim has been formulated, tested and verified over a radar area by Lovejoy and Austin (1979a). The application of this algorithm to rain amount estimation is discussed in Lovejoy and Austin (1979b). The main drawback of this technique is its limitation to daylight hours.

In the following, a revised version of that fundamental procedure which introduces the concept of probability of rain at a point derived from satellite data (here denoted by $P_{RS}$), has been applied to an area of the synoptic scale. The displacement of the $P_{RS}$ pattern has been determined for appropriate subareas by using a pattern recognition technique developed for the short-term radar precipitation forecasting scheme.

## 2. The test data

The data used in this work consist of SMS/GOES-E [Synchronous Meteorological Satellite/Geostationary Operational Environmental Satellite-East (North

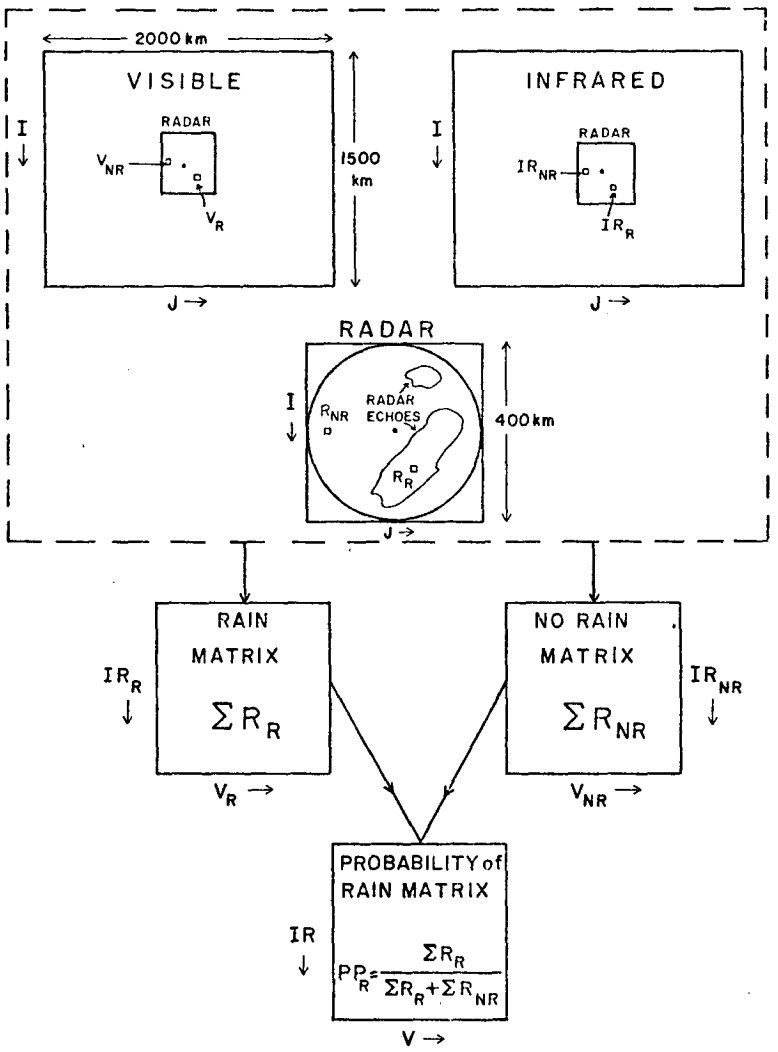


FIG. 1. Sketch illustrating the procedure in deriving probability of rain from satellite visible and infrared imagery colocated with radar data.

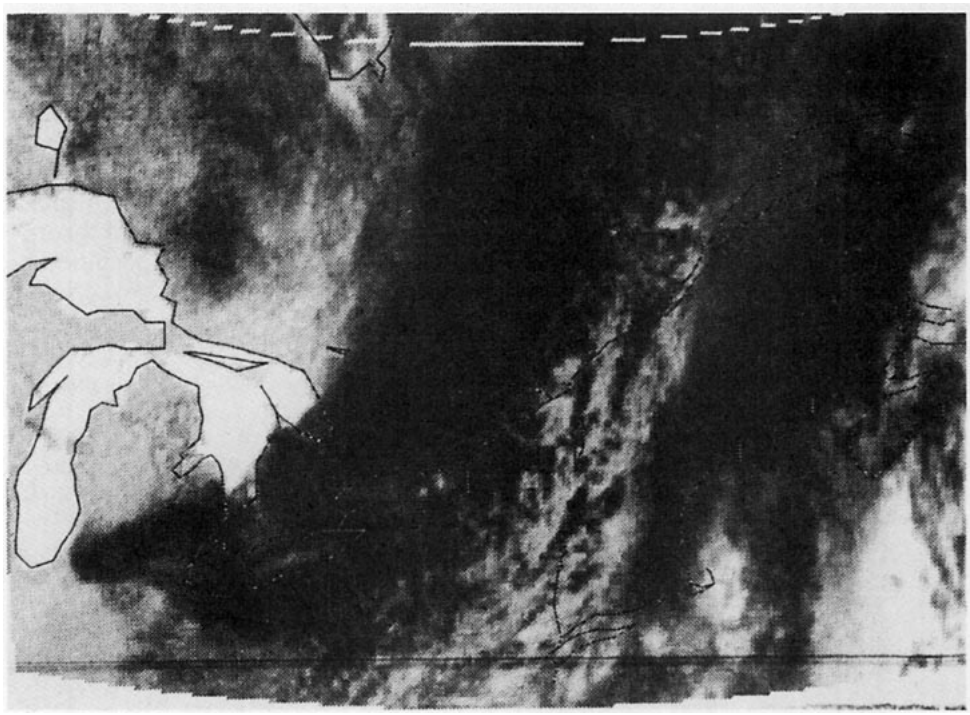

FIG. 2. Digital GOES-East visible satellite image of eastern Canada at 1830 GMT 2 June 1977, as produced by a continuous tone printer-plotter. The darker shades designate higher visible counts.

America)] digital images archived at 30 min intervals by the University of Wisconsin in Madison. Visible and infrared images are available with linear resolution of the order 1 km and 8 km, respectively, at subsatellite points.

Sequences of maps are needed to compute pattern displacement and this paper describes the analysis of data from only three days in June 1977. Corresponding radar data were obtained from the McGill weather radar, located 20 km west of Montreal. These were in the form of 3 km altitude CAPPI (Constant Altitude Plan Position Indicator) maps extending out to a range of 200 km.

## 3. Remapping of satellite data

On account of the inflexibility of most satellite display systems, one is often obliged to remap other data sets, e.g., radar and synoptic data onto satellite coordinates. Since in this work a pattern recognition technique is applied to two successive satellite pictures, it is highly desirable to use maps showing minimal areal and directional distortion. Moreover, since comparisons will be performed between the satellite-derived rain maps and synoptic charts, whether as part of a research analysis or, in real-time by a forecaster on duty, it is convenient to produce products on equivalent map projections. In mid-latitudes, a conic projection of the earth, true at two standard parallels, has been most commonly used by meteorologists. Using subroutines of the navigational model described by Smith and Phillips (1972) both visible and infrared images are remapped on a (187 × 255) array with a constant grid resolution of 8 km. This procedure is accomplished rapidly in a modest-size minicomputer.

## 4. Description of basic satellite rain-mapping technique

The fundamental algorithm consists of obtaining two bivariate frequency distributions from visible and infrared images, colocated with simultaneous radar data in order to discriminate between raining and non-raining clouds. The major steps of this procedure are sketched in Fig. 1.

The visible counts are crudely normalized by assuming the brightest 5% of the data correspond to infinitely thick clouds and observing the variation of this brightness level as a function of the time of day.

Remapped visible and infrared digital picture and the corresponding radar map form the data base. The radar enables us to identify the raining $R_R$ from the non-raining $R_{NR}$ points. For each $R_R$, the corresponding datum $V_R$ on the visible and $IR_R$ on the infrared image are located. The set $(IR_R,V_R)$ becomes the subscripts of a contingency matrix in which all the $R_R$ points are accumulated. Similarly, the pair $(IR_{NR},V_{NR})$ provides the coordinates of the no-rain matrix for all the radar echo-free points $R_{NR}$.

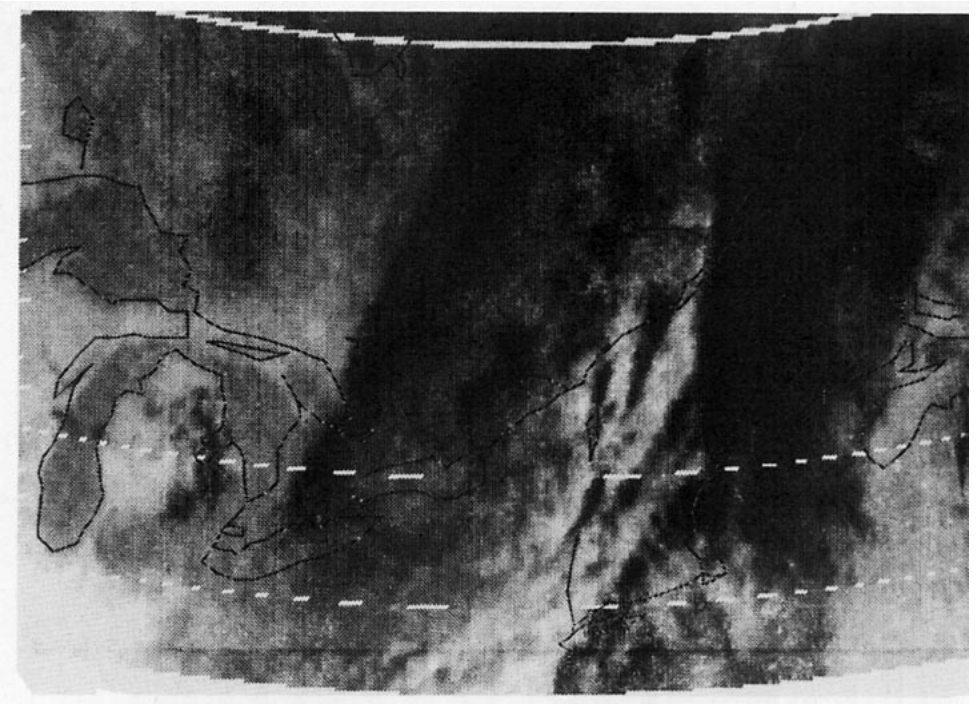

FIG. 3. Infrared image at 1830 GMT 2 June 1977. The darker areas indicate higher IR counts, i.e., colder temperatures.

These two arrays of bivariate frequency distribution in infrared-visible space are then combined to yield a probability of rain distribution as a function of infrared and visible values, expressed as

$$P_{RS}(\mathrm{IR,V}) = \frac{R_R(\mathrm{IR,V})}{R_R(\mathrm{IR,V}) + R_{NR}(\mathrm{IR,V})} . \quad (1)$$

$R_R$(IR,V) is the number of occurrences of rain with associated (IR,V) magnitudes and the denominator represents the total number of points in each (IR,V) interval. The above empirical relationship, derived from (IR,V) values within radar range is then assumed to apply over the entire domain of the satellite image. Thus, the underlying assumption used in extracting rain information from satellite data is that those clouds which are thick (i.e., of intense visible brightness) in comparison with their height (as inferred from the infrared counts) possess a greater probability of producing rain.

This entire process is illustrated by means of actual data. Figs. 2 and 3 are the digital GOES visible and infrared images at 1830 GMT 2 June 1977, as produced by a continuous tone printer-plotter of a minicomputer. The darker areas in the remapped visible image shown in Fig. 2 designate higher visible counts (thicker and/or highly reflective clouds), while those on the infrared picture (Fig. 3) indicate that the top of the emitting cloud is at high altitude. The white areas denote absence of data or locations where one or more lines of suspect raw data have been removed by a filter routine. The geography consists of a dark outline if the background is light and reverses to a white line on a black background. The echoes observed by the McGill radar are shown in Fig. 4. Only radar information within a range of 200 km and which is not contaminated by ground clutter, mountains or shadowing effects is incorporated in the analysis. Tables 1a and 1b provide

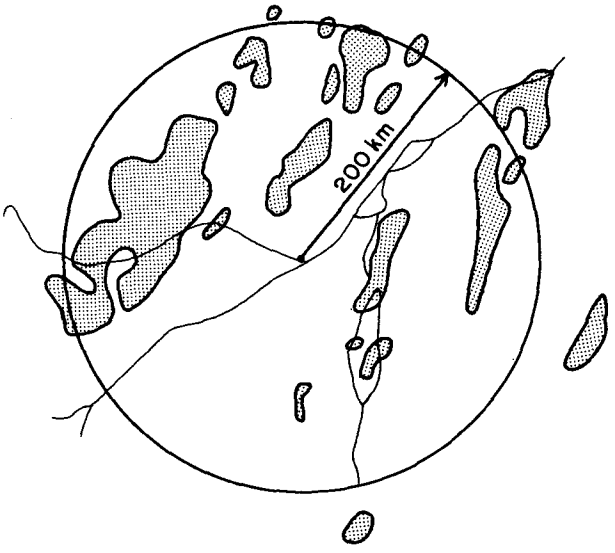


FIG. 4. Outline of the 0.5 mm $h^{-1}$ contour from the digital radar rainfall map at 1830 GMT 2 June 1977.

TABLE 1a. Bivariate frequency distribution in visible and infrared space of the "rain" grid areas for 1830 GMT 2 June 1977.

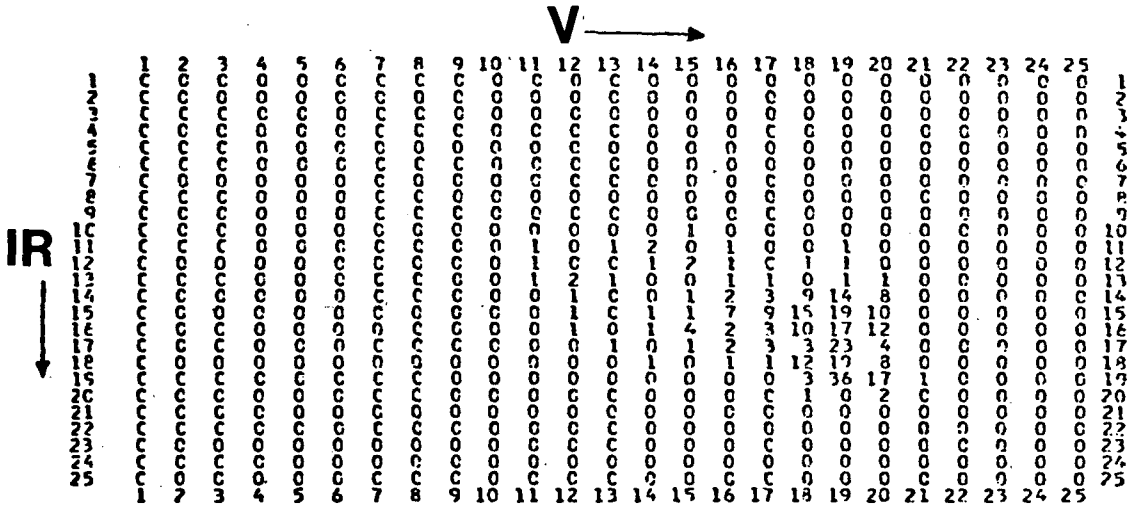


TABLE 1b. Bivariate frequency distribution in visible and infrared space of the "non-raining" grid areas for 1830 GMT 2 June 1977.

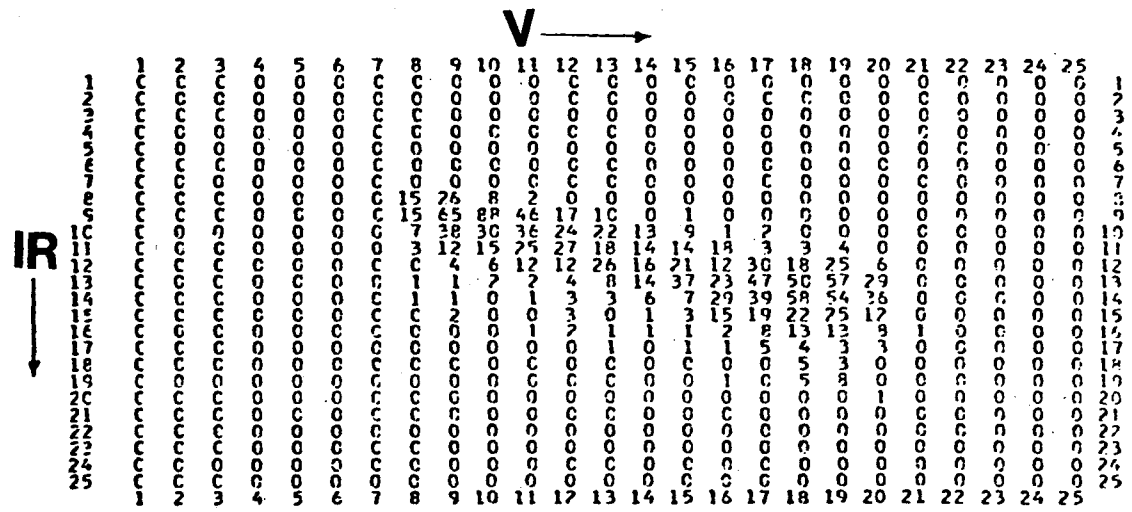


TABLE 1c. Percentage probability of rain distribution as a function of infrared and visible values. −1 indicates no data.

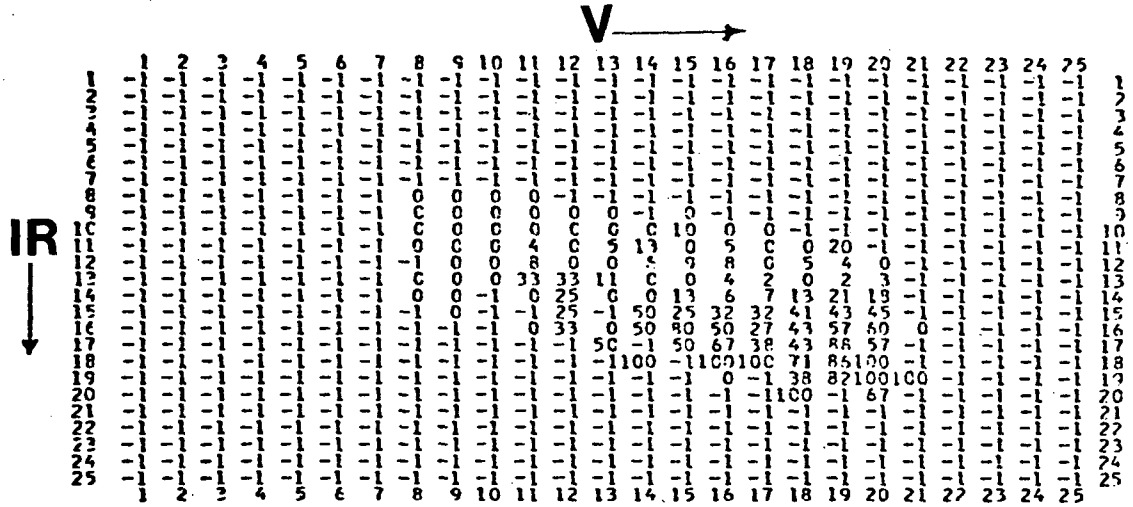

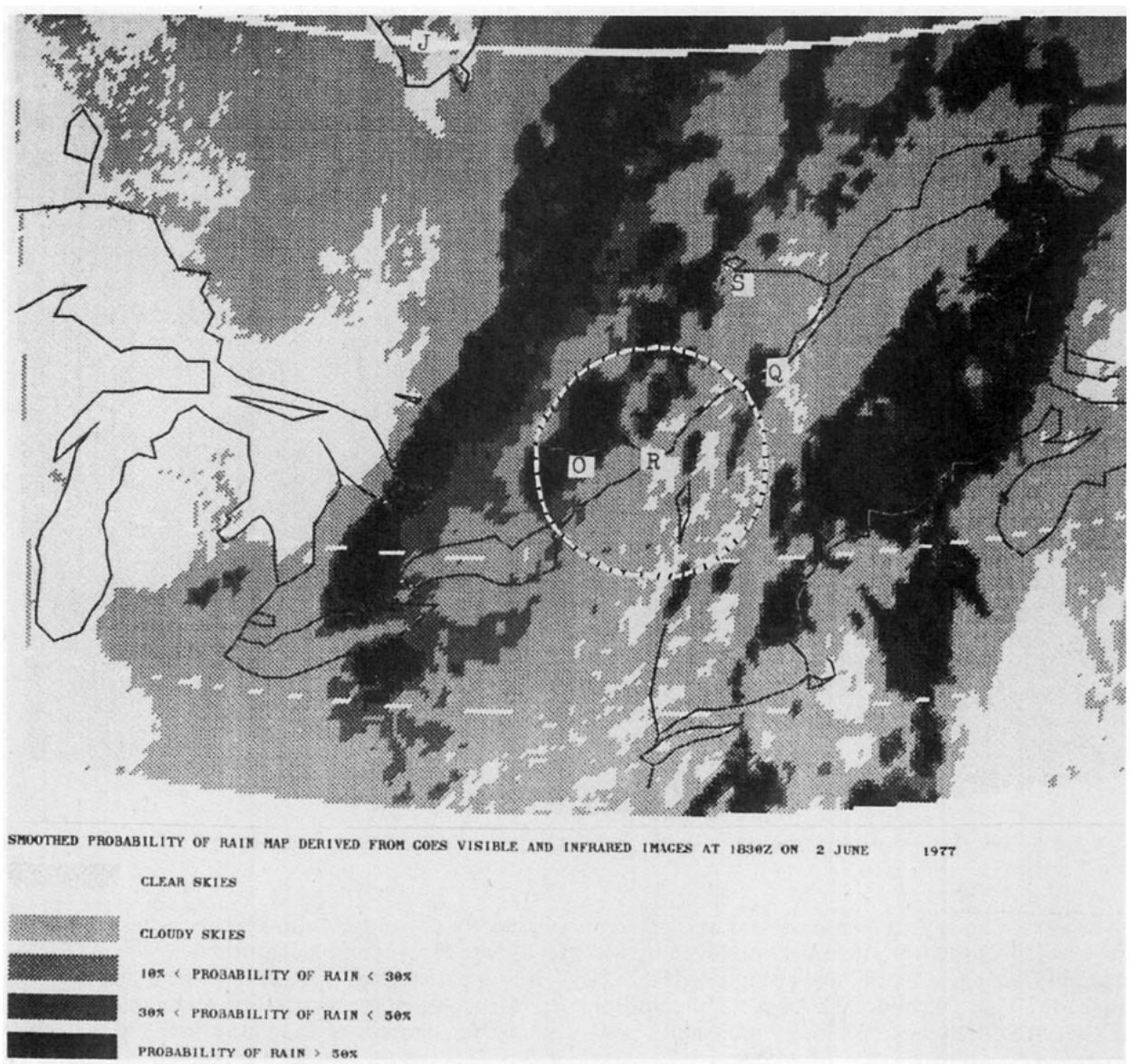


FIG. 5. Smoothed probability of rain map at 1830 GMT 2 June 1977, derived from GOES visible and infrared images. R: Radar, Q: Quebec City, O: Ottawa, S: Saguenay and Lake St-John, J: James Bay.

the frequency distributions of the raining and non-raining points, respectively, as a function of equally spaced visible and infrared levels. Application of Eq. (1) yields the percentage probability of rain values found in Table 1c.

After assigning a probability of rain value over the entire satellite map on the basis of Table 1c, and applying simple procedures for eliminating noise and map mismatch problems discussed in greater detail in Bellon (1979), a 5-point smoother with double weight on the center grid is applied. This step has the effect of adding spatial information and yields easily recognizable $P_{RS}$ contours. This smoother has been applied to all the maps with generally good results in the radar verified regions, and may be justified by the high meteorological correlation of regions ~10 km apart.

The ultimate result (the spatially smoothed probability of rain map from GOES visible and infrared images) is presented in Fig. 5. Five shades or levels can be distinguished:

| *Level* | *Characteristic* |
|---|---|
| 1 | clear skies defined as a normalized visible count, $c_{VIS} < 90$ |
| 2 | cloudy skies defined as $c_{VIS} \geq 90$ and $P_{RS} < 0.1$ |
| 3 | $0.1 \leq P_{RS} < 0.3$ |
| 4 | $0.3 \leq P_{RS} < 0.5$ |
| 5 | $P_{RS} \geq 0.5$ |

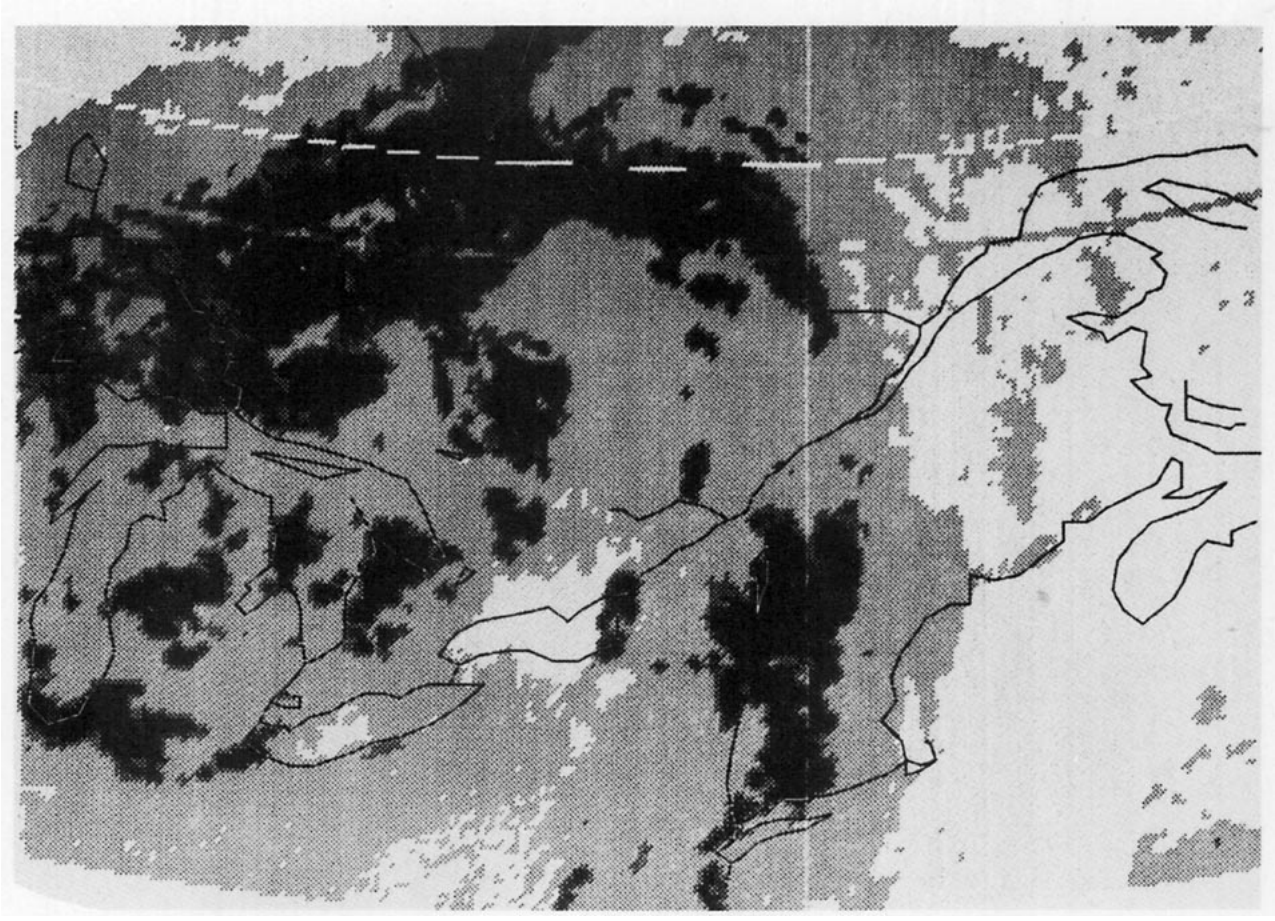

FIG. 6. Smoothed probability of rain map derived from GOES visible and infrared images at 1830 GMT 1 June 1977.

The cirrus and stratus components of the infrared and visible pictures are effectively removed by the bivariate frequency distribution technique. For example, the high infrared values over and south of the Gulf of St. Lawrence could be classified as rain-producing clouds by a single infrared threshold technique. However, the visible counts over this region reveal them to be relatively thin, probably cirrus fields. Hence, Fig. 5 indicates no probability of rain. Similarly, clouds with a relatively high visible albedo but lower infrared counts (i.e., of low altitude) are categorized as non-raining. Instances can be found by comparing Figs. 2, 3 and 5, particularly in southern Michigan and along the wide cloud band aligned from just east of James Bay to west of Lake Erie. It may be observed that along this band, the high infrared values exhibit a better correspondence with the rain areas of Fig. 5 than does the visible picture. Note that the radar echoes of Fig. 4 are substantially reproduced by the $P_{RS}$ map of Fig. 5.

## 5. Motion of satellite rain areas

In order that satellite rain maps be used as input to short-range forecasting schemes, the technique described earlier must produce rain zones which are sufficiently consistent in time so as to be trackable by a pattern recognition algorithm.

It is apparent that, to determine the motion of the $P_{RS}$ zones, a pattern recognition technique must be applied to subareas of the entire map. Hence, the (187 × 255) matrix has been sectioned into 16 subareas. Each consists of a (46 × 64) array, or 368 × 512 = 188 000 km². The SHARP program operates successfully in real-time over an area of about 132 000 km². Tracking of radar echoes over this area using a cross-correlation scheme has revealed a fairly uniform motion (Bellon and Austin, 1978). A larger area has been chosen for tracking of satellite rain zones since, as was expected, they are less consistent and exhibit less continuity in time than radar echoes. Equally important is the need for a proper balance between the temporal and spatial resolution and the characteristic scale length of the patterns. Only zones for which $P_{RS} \geq 0.3$ are considered. The weighting in computing the cross-correlation coefficient is as follows:

$$P_{RS} \geq 0.5 \quad 2 \text{ (weighting)},$$

$$0.3 \leq P_{RS} < 0.5 \quad 1 \text{ (weighting)},$$

$$P_{RS} < 0.3 \quad 0 \text{ (weighting)}.$$

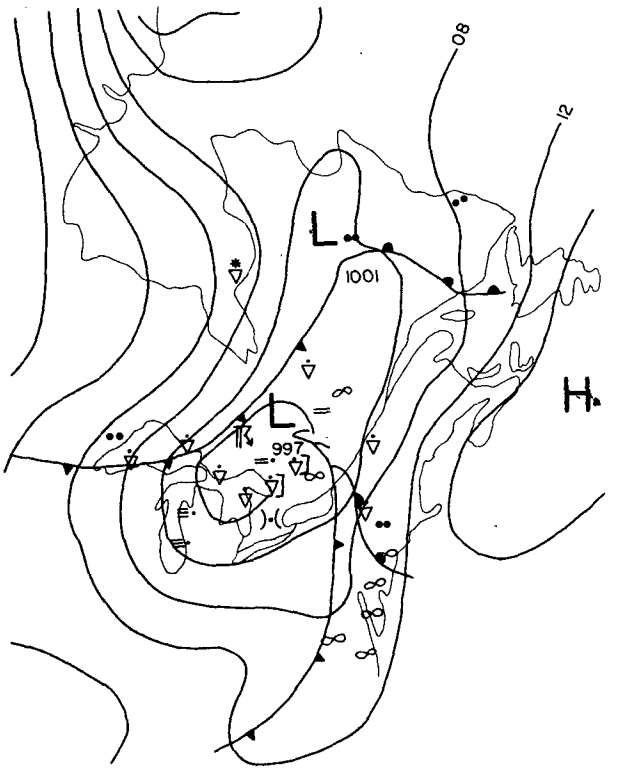


FIG. 7. Surface synoptic chart at 1800 GMT 1 June 1977 as analyzed by the Quebec Forecast Office.

A minimum of 1% coverage over the subarea is required before attempting the cross correlation of the probability of rain zones.

*a. Case 1 (1 June 1977)*

One of the six 30 min $P_{RS}$ maps forming the sequence of 1 June 1977 between 1730 and 2000 GMT is portrayed in Fig. 6. The surface synoptic chart at 1800 GMT, as analyzed by the Quebec Forecast Office, is given in Fig. 7. It shows a depression in central Quebec with a cold front trailing across through the northern Great Lakes. A low pressure system with a trowel, originating in the Mississippi Valley, and advecting warm, moist air, is converging toward the descending cold front.

The $P_{RS}$ zones of Fig. 6 are considered to be sufficiently consistent over the 2.5 h period. The patch south-southeast of Montreal is associated with the advancing warm front. With the exception of a developing Cb just east of Lake Ontario, the southern cold front is relatively inactive. The configuration of the rain pattern northwest of the Saguenay region seems to denote the presence of a warm front. While it is not analyzed on the synoptic chart, a steep temperature gradient, from high 20's to the teens, is observed at the surface. The rain area with a circular shape northwest of Ottawa coincides with the location of the low pressure center. The scat-

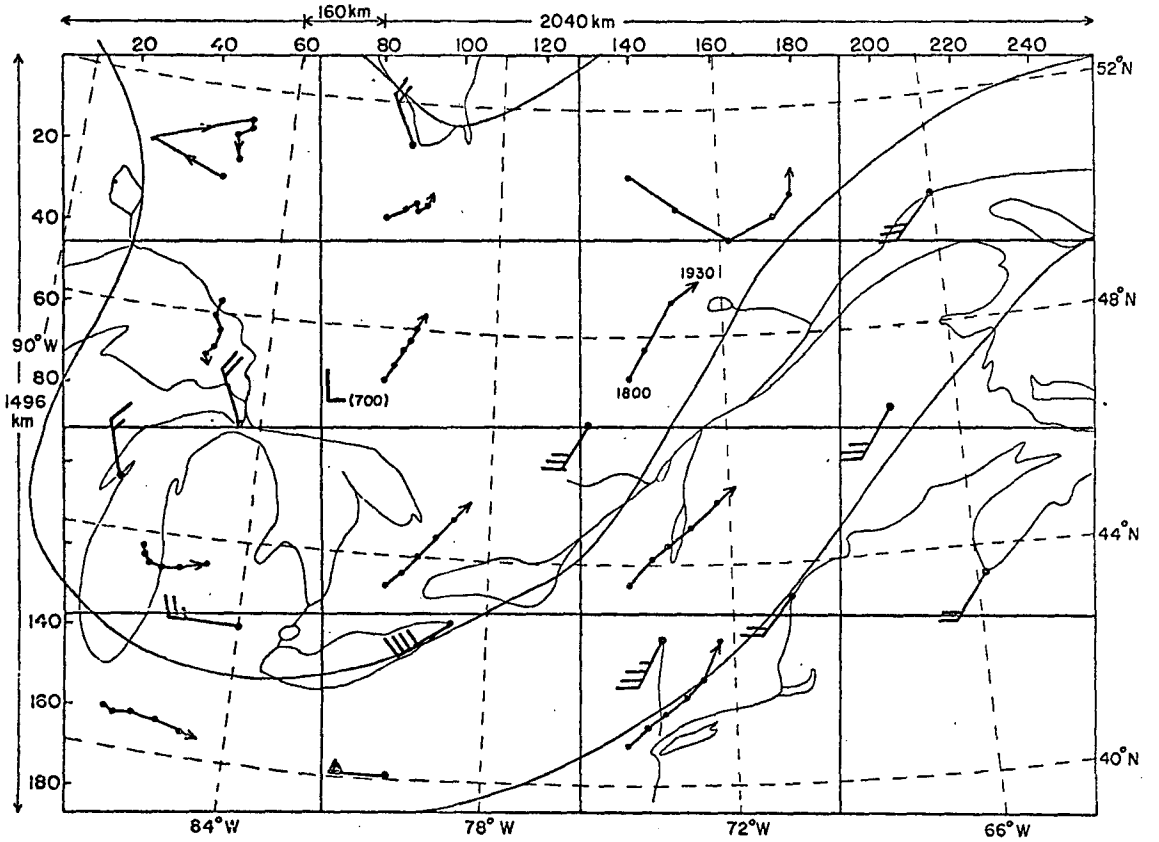


FIG. 8. Trajectories derived over each sub-area with sufficient "satellite echo" coverage for 1730–2000 GMT 1 June 1977.

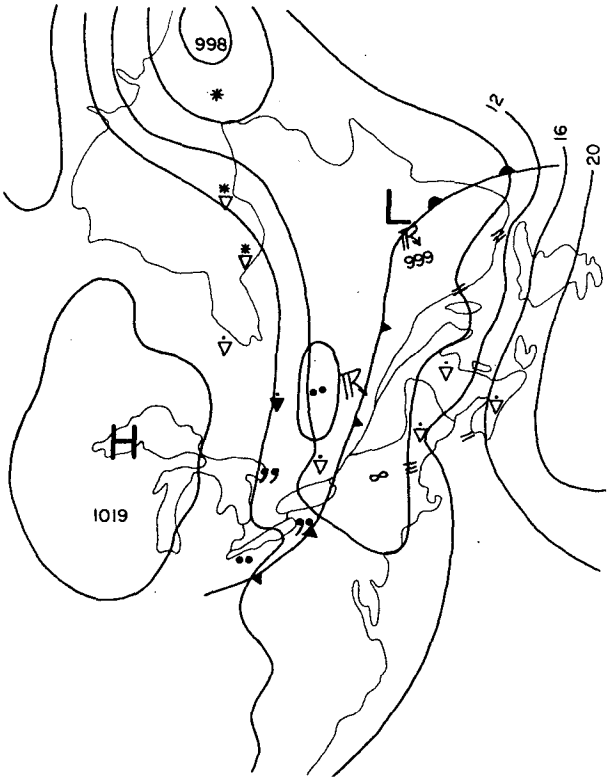


tered showers extending to southern Lake Michigan are associated with a lagging trough over the Great Lakes. The more extensive rain area is found at or behind the arctic cold front. When the significant surface observations were superimposed on the $P_{RS}$ contours of the 1800 GMT map, the comparison was found to be acceptable. A strict comparison could not be performed on account of drastic differences in the temporal and spatial scale between satellite data and synoptic charts.

The results of the tracking program for the sequence of case 1 are summarized in Fig. 8. The 30 min displacements, computed in fractions of grid lengths, have been summed to form a trajectory for each subarea. The 700 mb analysis for 2400 GMT, with the radiosonde wind data, has been added for visual comparison, since it is commonly associated with movement of mid-latitude precipitation areas (Harper and Biemers, 1958). Fig. 8 shows that the $P_{RS}$ zones on the southern section of the map have been correctly followed yielding a displacement which compares favorably with the 700 mb wind. Rain zones speeds of the order of 50 and 60 km $h^{-1}$

FIG. 9. Surface synoptic chart at 1800 GMT 2 June 1977 as analyzed by the Quebec Forecast Office.

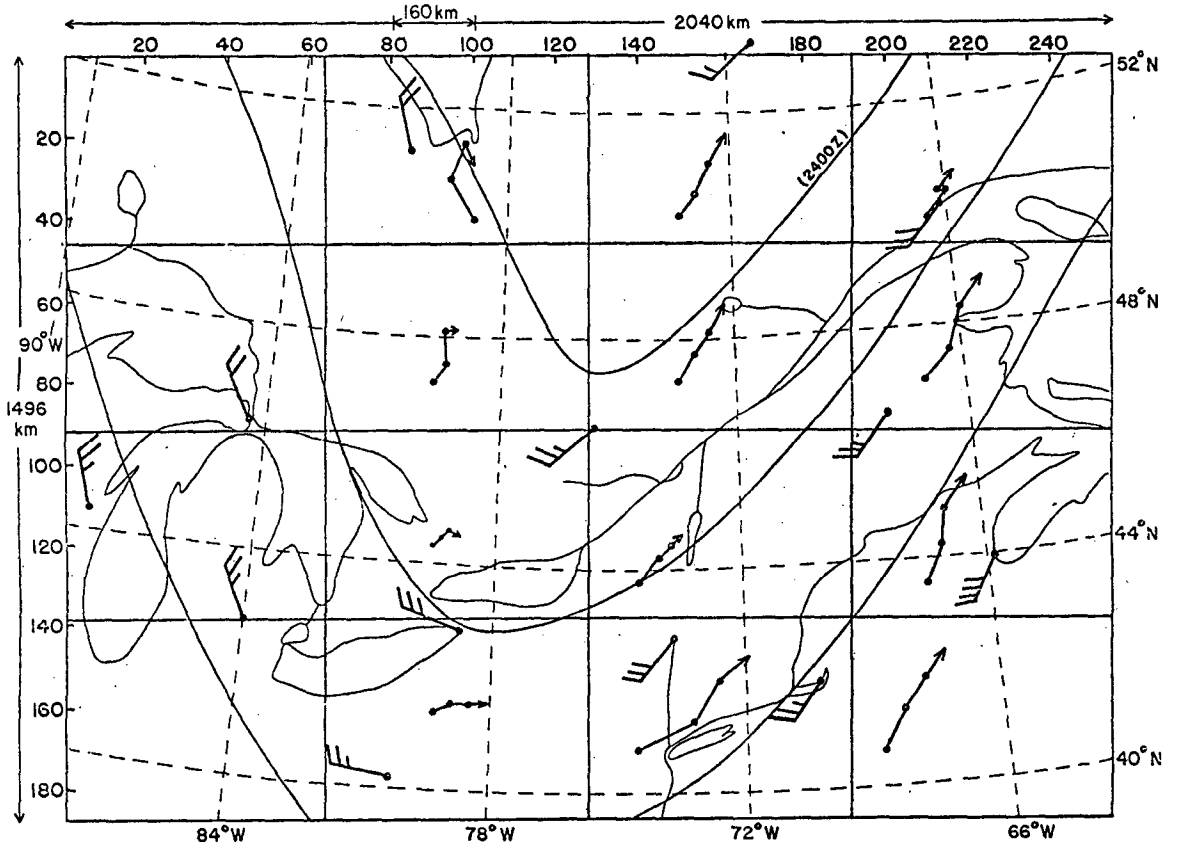


FIG. 10. Trajectories for 1730–1900 GMT 2 June 1977.

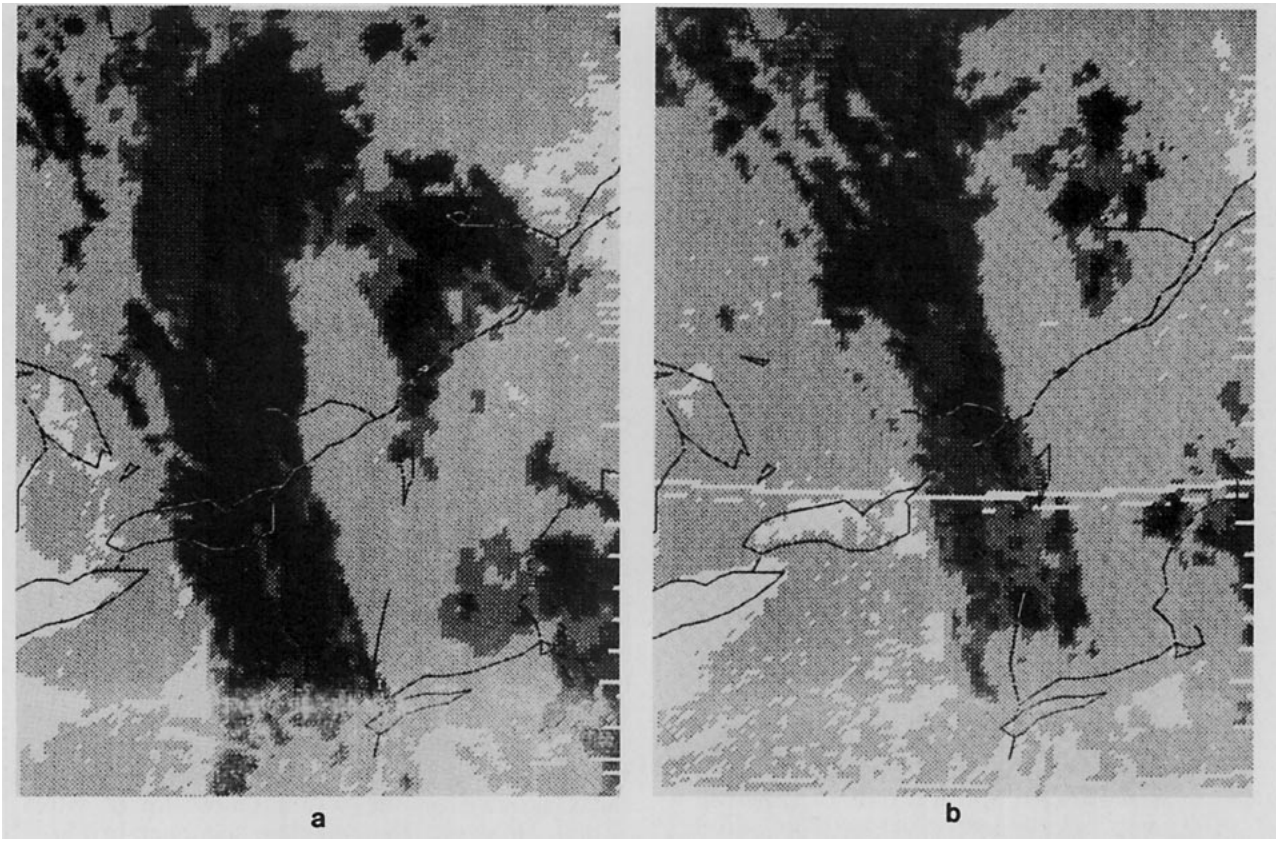


FIG. 11. Selected probability of rain maps for the sequence of 29 June 1977. (a) 1300 GMT, (b) 1530 GMT and (c) 1730 GMT.

correlate well with the wind velocity found ahead of the 700 mb trough.

In this region the linearity in both speed and direction augurs well for a short-term forecasting system based on pattern extrapolation. Behind the arctic front, or closer to the 700 mb center, lower speeds are calculated in accordance with upper level data but, as illustrated by subarea (3, 1) which includes the Michigan area, the expected passage of an upper front must be taken into account when performing a forecast by pattern advection. Development and dissipation of rain areas has not been included since our experience with radar data indicates that only a minimal advantage can be expected.

A disturbing aspect of Fig. 8 is the trajectories in the northern portion of the map. It is obvious that the first two calculated displacements for subareas (1, 1) and (1, 3) constitute spurious motion. These are caused by the absence of easily recognizable features, or by the creation of artificial ones arising from the arbitrary sectioning of patterns into subareas, or by a high percentage coverage as in (1, 2). Our field experience has revealed that coverage $> 40\%$ is as detrimental to a cross-correlation tech-

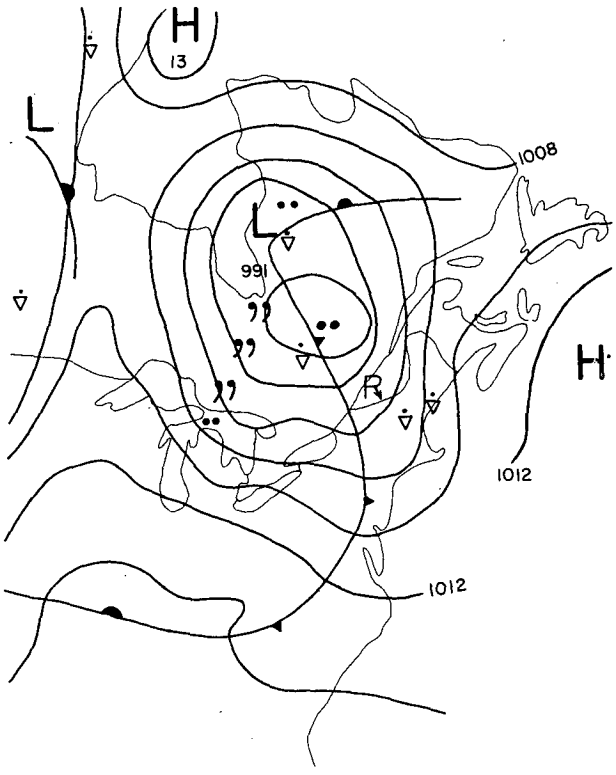


FIG. 12. Surface synoptic chart at 1700 GMT 29 June 1977 as analyzed by the Quebec Forecast Office.

nique as insufficient coverage, by underestimating the actual motion. An additional explanation for the erratic motion in subareas (1, 1) and (1, 3) is that the rain-determination algorithm, derived from radar data near 45°N latitude, may not be as stable in northern latitudes, yielding rain zones with edges which appear to advance or recede at unreasonable speeds. However, as was the case in the real-time operation of SHARP, certain criteria which will not be dealt with here, can be introduced which will reject apparently unacceptable displacements.

*b. Case 2 (2 June 1977)*

One of the $P_{RS}$ maps of this short 1.5 h sequence between 1730 and 1900 GMT was presented in Fig. 5. The 1800 GMT surface analysis (Fig. 9) shows that the cold front, which 24 h earlier was stretching from James Bay to north of Lake Superior, has descended in a rotational movement south of Lake Erie and Lake Ontario. The depression which originated from the southwest is completely amalgamated into the cold front which is now of a more convective character. Smaller disturbances, analyzed on subsequent charts, have also developed along the front. The wave crest associated with the southwest low has meanwhile moved into Maine and New Brunswick (from the 1200 GMT analysis). The rainbands associated with these two principal systems are well delineated in Fig. 5. Fig. 5 also reveals that two lines are connected with the cold front.

The first one, elongated from north of Lake St. John through Ottawa and south of Lake Erie, coincides with the arctic front position. In addition, a wider and more continuous band of precipitation is located 300 km behind it. In the relatively clear area between the precipitation over Ontario and near the Maritimes, intense solar heating induced the formation of localized thunderstorms arranged in short lines just east of Montreal and near Quebec City. The formation, development and displacement of these convective storms can be observed from the complete set of $P_{RS}$ maps.

The trajectories from the four 30 min maps have been derived as described earlier. Correlation with the 700 mb wind speed at 2400 GMT, shown in Fig. 10, is generally good, with a notable exception occurring in box (1, 2) near James Bay. Some discrepancies just west of the trough can be accounted for by the time difference between the trajectories and the radiosonde data. Attention is directed to the line of precipitation over the Atlantic east of Cape Cod with a trajectory toward Nova Scotia—see box (4, 4). The extent of this precipitation zone will likely be incomplete, even as determined by a weather radar situated on the southernmost tip of Nova Scotia. However, the complete sequence of Fig. 5 and the trajectory display of Fig. 10 can provide an adequate forecast for the arrival and duration of precipitation over that province.

*c. Case 3 (29 June 1977)*

This case study consists of the longest sequence, 1300–1730 GMT. However, the longitudinal extent of the satellite data (Fig. 11) is approximately half the size of maps seen so far. The synoptic situation at 1700 GMT depicted in Fig. 12 is characterized by a deep low pressure system east of James Bay with a cold front as indicated. Fig. 11 illustrates very well the passage of the rain area over Montreal. This main band precedes the cold front and limits its activity to latitudes north of New York City. In this case, the comparison with surface observations was very good. The showers in the vicinity of Maine are correctly identified on the $P_{RS}$ maps. The difference in resolution between satellite and synoptic maps is brought into sharp focus by the synoptic analysis near the Saguenay region. Both satellite and surface reports indicate precipitation near Lake St. John and at a station ~200 km to the west-northwest. While in the synoptic analysis rainfall is assumed between the two sites, the satellite data suggest this was not the case.

The map of trajectories in Fig. 13 is limited to eight subareas. The 700 mb data are from 1200 GMT.

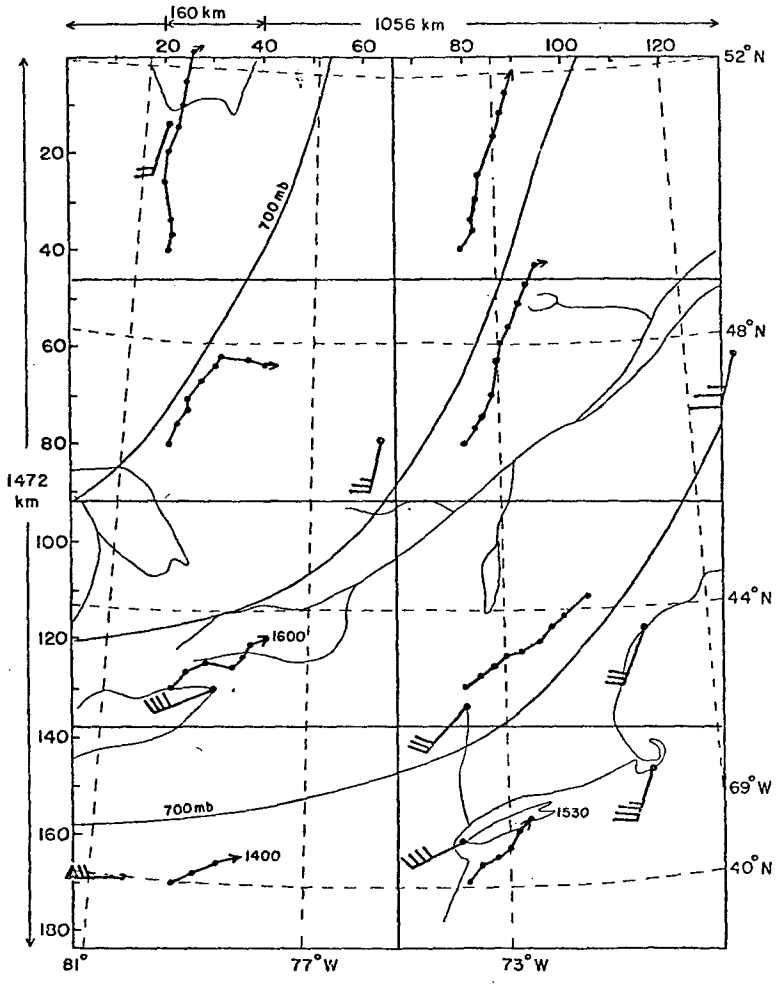


FIG. 13. Trajectories for 1300–1730 GMT 29 June 1977.

Vectors in the southern latitudes are from a west-southwest or southwest direction while motion just ahead of the depression is southerly. Note the shift in the motion in box (2, 1) following the passage of the cold front.

## 6. Conclusions

The production of GOES-based satellite rain maps has been extended from the radar region ($\sim 10^5$ km$^2$) to all of eastern Canada ($\sim 2 \times 10^6$ km$^2$). The accuracy of the maps has been improved by smoothing in order to add spatial information to the existing IR and visible magnitude information. These rain (or rather probability of rain) maps were shown to be sufficiently spatially and temporally homogeneous as to allow tracking similar to that of radar echo areas. The resulting trajectories showed excellent agreement with 700 mb synoptic wind fields. The probability of rain contours also compared favorably with surface synoptic reports.

As a result of this work and other more detailed analyses described in Bellon (1979), an operational version of this scheme called "Rainsat" has been devised and is expected to be in full real-time operation in summer 1981. It is realized that the work reported here only represents a small step toward improved very short-range forecasting; we believe that the immediate implementation of a prototype procedure will speed up the evolution of a complete system based on experience and results from a large number of cases.

*Acknowledgments*. Much of the data analysis system described here was developed by Ms. Alamelu Kilambi and Dr. S. Radhakant.

The strong support of the Atmospheric Environment Sevice through the good offices of its Assistant Deputy Minister, Dr. A. E. Collins, and the Chief of the satellite Data Lab, Mr. E. G. Morrissey, is gratefully acknowledged. Helpful discussions with Drs. Don Wylie, Fred Mosher and Dave Martin, of the University of Wisconsin, and Dr. Keith Browning and Mr. C. G. Collier, of the Radar Group of the British Meteorological Office, are also appreciated.

## REFERENCES


Austin, G. L., and A. Bellon, 1974: The use of digital weather radar records for short-term precipitation forecasting. *Quart. J. Roy. Meteor. Soc.*, **100**, 658–664.

Bellon, A., 1979: The development of a real time automated system for short range precipitation forecasting using combined radar and satellite data. Final Report for AES (DSS) Contract 0SU78-00056 42 pp. [Available from Stormy Weather Group, McGill University, Montreal, Quebec, Canada.]

——, and G. L. Austin, 1978: The evaluation of two years of real time operation of a short-term precipitation forecasting procedure SHARP). *J. Appl. Meteor.*, **17**, 1778–1787.

Browning, K. A., 1979: FRONTIERS Plan: A strategy for using radar and satellite imagery for very-short-range precipitation forecasting. *Meteor. Mag.*, **108**, 161–184.

Griffith, C., W. L. Woodley, G. Gruber, D. W. Martin, J. Stout and D. N. Sikdar, 1978: Rain estimation from geosynchronous satellite imagery—visible and infrared studies. *Mon. Wea. Rev.*, **106**, 1153–1171.

Gruber, A., 1973: Estimating rainfall in regions of active convection. *J. Appl. Meteor.*, **12**, 110–118.

Harper, W. C., and J. G. D. Beimers, 1958: The movement of precipitation belts as observed by radar. *Quart. J. Roy. Meteor. Soc.*, **84**, 242–249.

Lovejoy, S., and G. L. Austin, 1979a: The delineation of rain areas from visible and IR satellite data for GATE and mid-latitudes. *Atmosphere-Ocean*, **17**, 77–92,

——, and ——, 1979b: The sources of error in rain amount estimating schemes from GOES visible and IR satellite data. *Mon. Wea. Rev.*, **107**, 1048–1054.

Martin, D. W., and W. D. Scherer, 1973: Review of satellite rainfall estimation methods. *Bull. Amer. Meteor. Soc.*, **54**, 661–674.

Reynolds, D. W., and E. A. Smith, 1979: A detailed analysis of composited digital radar and satellite data. *Bull. Amer. Meteor. Soc.*, **60**, 1024–1037.

——, M. L. Brown, E. A. Smith, and T. H. Von der Haar, 1978: Cloud type separation by spectral differencing of image pairs. *Mon. Wea. Rev.*, **106**, 1214–1218.

Sanders, F., 1979: Trends in skill of daily forecasts of temperature and precipitation, 1966–78. *Bull. Amer. Meteor. Soc.*, **60**, 763–769.

Scofield, R. A., and V. J. Oliver, 1977: A scheme for estimating convective rainfall from satellite imagery. Tech. Memo. NESS 86, NOAA, Washington, DC, 47 pp.

Smith, E. A., and D. R. Phillips, 1972: Automated cloud tracking using precisely aligned digital ATS pictures. *IEEE Trans. Comput.*, **C-21**, 715–729.

Stout, E. J., D. W. Martin and D. N. Sikdar, 1979: Estimating GATE rainfall from geostationary satellite images. *Mon. Wea. Rev.*, **107**, 585–598.

Wylie, D. P., 1979: An application of a geostationary satellite rain estimation scheme to an extrapolation area. *J. Appl. Meteor.*, **18**, 1640–1648.